© Japanese Society of Electron Microscopy
Journal of Electron Microscopy **50(3)**: 227–233 (2001)

Full-length paper

On the origin of transverse incoherence in Z-contrast STEM

Brian Rafferty[1,2], Peter D. Nellist[3,4,*] and Stephen J. Pennycook[1]

[1]Oak Ridge National Laboratory, Solid State Division, P.O. Box 2008, Oak Ridge, TN 37831-6030, USA and [3]Nanoscale Physics Research Laboratory, School of Physics and Astronomy, Birmingham University, Birmingham B17 8DJ, UK

Present address: [2]Leica Microsystems Lithography Ltd, Clifton Road, Cambridge CB1 3QH, UK and [4]Nion Co., 1102 8th St, Kirkland, WA 98033, USA

[*]To whom correspondence should be addressed. Fax: +1-425-739-0312; E-mail: nellist@nion.com

Abstract We use a Bloch wave approach to further investigate the origins of the incoherent nature of Z-contrast imaging using an ADF detector in a STEM. We discuss how, although at high angles the collected electrons will be mostly thermally scattered in addition to the elastic scattering, it is not the thermal scattering that destroys the coherence, rather the combination of the large detector with the high-angle elastic scattering. This incoherent nature of the elastic scattering arises through the filtering of the 1s-type Bloch states by the detector geometry. We show that it is this filtering that renders an atomic column an independent scatterer insensitive to the configuration of neighbouring columns. It also makes the image contrast insensitive to the effects of beam spreading onto neighbouring columns as the probe propagates through the crystal. We also discuss the implications of this for previous calculations of the intensity of Z-contrast images.

Keywords scanning transmission electron microscopy, Z-contrast, ADF, Bloch waves, thermal diffuse scattering, imaging theory

Received 27 December 2000, accepted 19 March 2001

Introduction

Annular dark-field (ADF) images taken in the scanning transmission electron microscope (STEM) of zone-axis orientated crystals show no contrast reversals with sample thickness. These images have been termed *incoherent* and interpreted as direct structure images of the atomic column positions, each column acting as an independent scattering centre whose strength is controlled by parameters such as the column's average atomic number and its thickness [1–5]. In characterizing the images as incoherent there has been much confusion as to what is to be understood by this term. In this context, incoherent means that we can describe the image intensity as the convolution between the intensity of the electron probe and an object function; each atomic column acting as an independent scattering centre, thus negating the problems experienced in conventional coherent high-resolution transmission electron microscopy (HRTEM) due to dynamical diffraction effects. With ADF imaging we break the transverse coherence between atomic columns, allowing one to simply interpret bright spots in the image as atomic-columns in the crystal structure. This is the key property of ADF imaging for when analysing an unknown grain boundary or interface it gives instant access to the projected atomic configuration. This allows us to concentrate on acquiring and interpreting electron energy loss (EEL) spectra and fine structure from selected columns in known locations.

The original proposal for incoherent imaging in a STEM [6] made the reasonable assumption that at high enough angles, the scattering would be dominated by incoherent thermal diffuse scattering (TDS), thus rendering the image incoherent. Pennycook and Jesson [7,8] quantified this approach by assuming that the TDS to the ADF detector could be treated as coming from incoherent scattering cross-sections at the atom sites. Taking into account the dynamical scattering of the elastically scattered electrons as they propagate through the crystal to compute the electron intensity within the crystal, they integrated the electron intensity over the incoherent cross-sections to derive the total ADF signal.

Experimentally, however, it is found that incoherent structure images of the crystal are formed even when the detector collects zero-order Laue zone (ZOLZ) discs, indicating that TDS is not a prerequisite for incoherent imaging. Indeed, later

work by Jesson and Pennycook [9] incorporating more realistic phonon scattering into a kinematical model showed that correlations between the thermal vibrations of nearby atoms mean that the coherence envelopes arising from TDS can be several atoms wide. It is, therefore, clear that TDS itself is not enough to break the coherence of the scattering from neighbouring atoms. Using kinematical [10] or thin specimen [11] approximations it was, therefore, shown that coherent elastic scattering could lead to the coherence being broken in the directions perpendicular to the beam.

More recently, Nellist and Pennycook [12] have extended this approach to demonstrate how even using a dynamical calculation with no absorption, the geometry of the ADF detector breaks the coherence transverse to the beam. The use of a Bloch wave calculation in this approach, while not practical for the analysis of defects, does allow the physics of the formation of the incoherent image from such elastically scattered electrons to be understood more clearly. Gaining an understanding of the physics of the image formation process is an important step, since it reveals what needs to be modelled carefully and what can be approximated in any full-blooded ADF simulation package.

In this paper we show further results from the Nellist and Pennycook approach, and discuss their implications for the formation of the ADF image. We start by discussing why considering only elastic scattering is an important step, even when the actual intensity arriving at the ADF appears to be mostly TDS. We then present results from simulations of InAs in the <110> orientation that show why the spreading of the beam into neighbouring columns as the probe propagates through the crystal (also known as column cross-talk) does not lead to coherent interference effects between the columns, and that removal of complete columns does not affect the intensity of their neighbours in the image. We also discuss how this approach allows greater understanding of the variation of intensity with thickness, and the important differences between this approach and the Pennycook and Jesson approach.

Bragg scattering and thermal diffuse scattering in ADF images

As the electrons propagate through the crystal they can be multiply elastically scattered by the potential of the atoms in the crystal, which is well described by the dynamical theory of electron scattering [13]. They can also be scattered by phonons, in which the momentum and energy of the fast electron is changed by the momentum and energy of the phonon that is being destroyed or created. Although the energy change of the fast electron due to the phonon is small (similar to room temperature thermal energies), it is enough to destroy interference effects between the thermally scattered electron and the elastically scattered electrons or other thermally scattered electrons. It is for this reason that TDS is often described as being incoherent scattering.

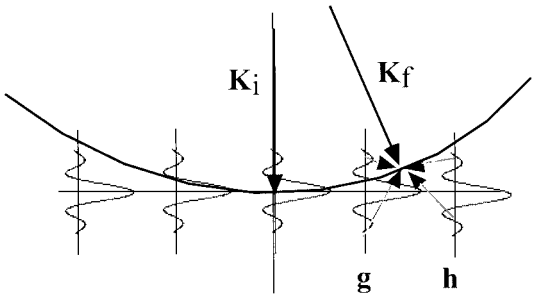

Fig. 1 The grey arrows depict scattering by phonons in addition to elastic scattering into a final wavevector, K_f. The phonons provide further integration in intensity in both the transverse and longitudinal directions.

To understand the role of TDS in the formation of the ADF image, it is instructive to compare typical scattering angles of dynamical elastic versus phonon scattering. The multiple elastic scattering (from even an individual column) can result in electrons with high enough transverse momentum that they can be scattered over many reciprocal lattice vectors. This can be evidenced by the strengths of the higher order Fourier components of the 1s states in a Bloch wave calculation of dynamical scattering, which show that the electrons channelling down the atomic columns close to the nuclei attain extremely high transverse momenta from the multiple elastic scattering. Phonons, however, have wavelengths that range from a lattice spacing too much longer than a lattice spacing, with the number distribution of phonons being greater towards the longer wavelength phonons. The typical momentum of phonons is, therefore, reciprocal lattice spacing or less, and is much smaller than typical momenta transferred by elastic scattering.

It is, therefore, possible to thinking of TDS as being the blurring of the higher angle Bragg diffracted beams by phonon scattering, with the blurring function being given by the distribution of phonon momenta (Fig. 1). Such an analysis has several important consequences. If we were relying on phonon scattering alone to break the coherence by using a small detector at high angle, as far as transverse coherence is concerned it would be equivalent to computing for a stationary lattice with a detector size comparable to typical phonon momenta (about a reciprocal lattice vector). Such a detector would not be large enough to break the coherence between neighbouring atoms, which requires a detector with dimensions of several times a reciprocal lattice vector. Thus, phonon scattering alone cannot break the coherence between neighbouring atoms, as shown previously [9]. For a large ADF detector with dimensions of several reciprocal lattice vectors, the redistribution of intensity by the transverse components of the momenta of the phonons is not relevant since the detector is so much larger than phonon momenta. The physics of the breaking of the transverse coherence can only be understood by modelling the detection of scattering from a stationary lattice by a large detector, which is the approach taken in this paper.

Figure 1 illustrates how the component of the phonon momenta parallel to the beam also provides an effective blurring in the longitudinal direction. It is this blurring that leads to the reduction in coherence in the longitudinal direction, which is broken only inefficiently by the detector geometry. Since the majority of phonon wavelengths are long, there is still some coherence between nearby atoms in the same column leading to a non-linear dependence of the image intensity on thickness.

The phonons also allow the ZOLZ reciprocal lattice points to be effectively coupled to the Ewald sphere to form the TDS. This coupling is probably the explanation of why the HOLZ contribution to the ADF image can and has been neglected in previous studies [8,14], which is important since it is well known that HOLZ contributions will not give transverse incoherence [15] because such reflections are only excited over narrow ranges of angles in the incident cone of illumination.

Bloch wave model

Using the formulation developed by Nellist and Pennycook [12], it can be shown that the Fourier transform of the ADF image for the case of scattering from a stationary lattice of thickness z is

$$\tilde{I}(\mathbf{Q}, z) = \int \left\{ \begin{array}{l} A(\mathbf{K}_i)A^*(\mathbf{K}_i + \mathbf{Q}) \times \\ \sum_{j,k} \Phi_0^{(j)*}(\mathbf{K}_i)\Phi_Q^{(k)}(\mathbf{K}_i) \sum_g D_g \Phi_g^{(j)}(\mathbf{K}_i)\, \Phi_g^{(k)*}(\mathbf{K}_i) \\ \times \exp[-2\pi i z(k_z^{(j)}(\mathbf{K}_i) - k_z^{(k)}(\mathbf{K}_i))] \end{array} \right\} d\mathbf{K}_i \tag{1}$$

where $\mathbf{K}_i$ is the transverse component of an incident partial plane-wave in the illuminating convergent beam, $\Phi_{\mathbf{g}}^{(j)}(\mathbf{K}_i)$ is the $\mathbf{g}$ Fourier component of the jth Bloch wave solution, whose eigenvalue gives a longitudinal component of wavevector of $k_z(\mathbf{K}_i)$, $D_{\mathbf{g}}$ is unity if a Bragg beam is collected by the ADF detector, zero otherwise.

Equation (1) is a complete reciprocal space picture that reveals the physics behind the scattering and formation of a Z-contrast image. The image contrast at a spatial frequency $\mathbf{Q}$ arises from the interference between partial plane-waves in the objective aperture that have transverse components of wavevectors separated by $\mathbf{Q}$ (Fig. 2). These two partial plane-waves each excite a set of Bloch states, represented by the sum over j and k, and interference can occur between the scattering into the same Bragg beam, $\mathbf{g}$. Thus, if we do not have a beam convergence semi-angle that is at least half the distance between neighbouring reciprocal lattice points (which would correspond to overlapping discs in a convergent beam diffraction pattern), there will be no image contrast as the probe is scanned across the sample.

In eq. (1) we have left in the explicit dependence on transverse component of wavevector of the incident partial plane-waves of the Bloch states and their eigenvalues. If we consider non-dispersive states, such as the highly localized 1s-type

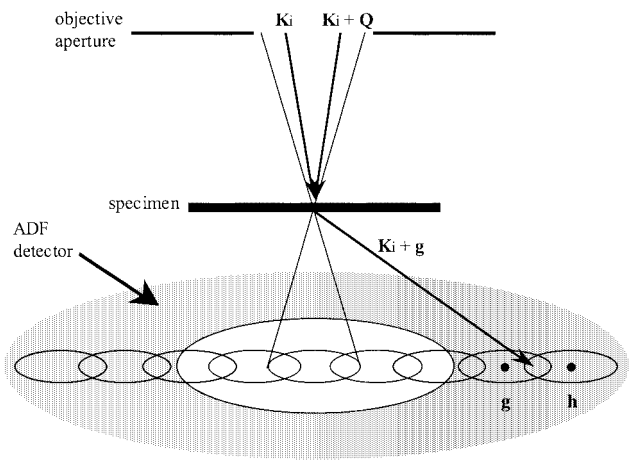

Fig. 2 The scattering geometry for ADF imaging in the STEM.

Bloch states, then this dependence is extremely weak and all the Bloch state terms can be taken outside of the integral over $\mathbf{K}_i$. We then have in reciprocal space the product between the autocorrelation function of the aperture function (the Fourier transform of the real-space probe intensity) and an object function containing all the information about the sample. Thus, the image intensity in real-space is the convolution between the probe intensity and an object function; we have exposed the source of the incoherent nature of a Z-contrast image, provided that non-dispersive states are the dominant contributing states to the image.

Another interesting feature of eq. (1) is that the sum over the detector function only involves two other terms. The other two are the $\mathbf{g}$ plane wave components of the two sets of Bloch waves excited by the pair of partial plane-waves in the incident cone. These terms can be replaced by a single value,

$$C_{jk}(\mathbf{K}_i) = \sum_g D_g \Phi_g^{(j)}(\mathbf{K}_i)\Phi_g^{(k)*}(\mathbf{K}_i) \tag{2}$$

which for $j = k$ terms is a measure of the amount that each Bloch state, j, contributes to the detector in reciprocal space. Bloch states that are spatially highly localized will have large high-angle Fourier components and, thus, contribute strongly to the C_{jj} term; it is through this term that the ADF detector acts as a filter for highly localized 1s-type Bloch states.

We can see from the above equations that the Bloch states interfere with one another in a rather complicated way as a function of thickness. However, we can separate out thickness independent 'self-terms' ($j = k$) and thickness dependent 'cross-terms' ($j \neq k$). At zero thickness, these sets of terms are equal to and opposite each other, resulting in zero intensity. As the thickness increases, the phase factor in eq. (1) will destroy the constructive, in-phase addition of all the cross-terms, weakening the contribution from these terms and leaving the self-terms to dominate the image contrast. We can now define a thickness independent residual object function (ROF) as,

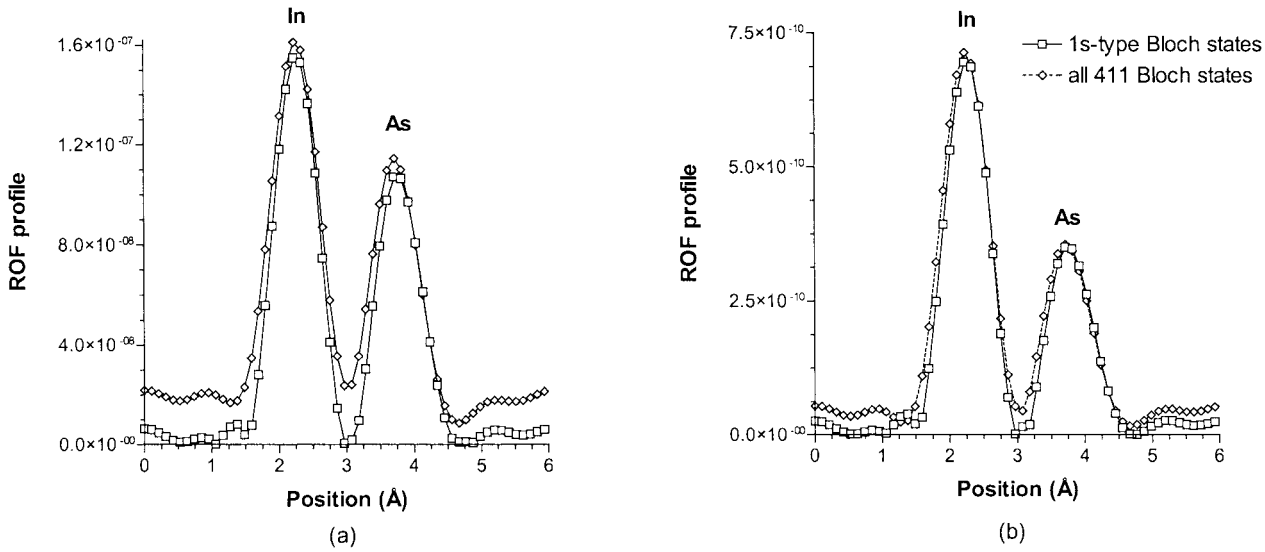

Fig. 3 ROF profiles across the InAs 'dumb-bell' structure for just the 1s-type Bloch states and all Bloch states for (a) 26 mrad and (b) 60 mrad inner detector angle.

$$\tilde{O}(\mathbf{Q}, \mathbf{K}_i) = \sum_j C_{jj}(\mathbf{K}_i)\Phi_0^{(j)*}(\mathbf{K}_i)\Phi_Q^{(j)}(\mathbf{K}_i) \qquad (3)$$

which is simply a sum over normalized Bloch waves weighted by their excitation coefficient and their detector filtering factor $C_{jj}(\mathbf{K}_i)$. If the sum is dominated by non-dispersive 1s states such that the dependence of eq. (3) on $\mathbf{K}_i$ is negligible, the Z-contrast image intensity is then the convolution between the real-space representation of the ROF and the real-space probe intensity.

Calculation results

1s-type Bloch state filtering

Bloch wave simulations were carried out at 300 kV for the <110> orientation of InAs (a = 6.06 Å). Calculations including 411-beams were carried out for a single incident partial plane-wave vector parallel to the optic axis. It has been shown elsewhere [16] that the 1s-Bloch states contributing to the ROF have a weak dependence on incident partial plane-wave orientation; consequently, there was no need to repeat the calculations for all incident partial plane-wave directions.

Figures 3a and 3b show the profiles across the classic 'dumb-bell' structure of the ROFs using just the 1s-type Bloch states and all 411 Bloch states for detector inner angles of 26 and 60 mrad, respectively. It can be clearly seen that the intensity of the peaks in the ROF are dominated by the contribution from the 1s-type Bloch states; the other 409 states contributing only to the tail regions of the column positions. But why is it that the 1s-type Bloch states dominate so strongly given that they are not the most excited states in the crystal? Table 1 shows the excitation coefficients and the filtering factors, C_{jj}, for the two inner detector angles for the first ten Bloch states. It can be seen that the 1s-type states do not have the strongest excitations, in fact the In 2s-type state has an excitation ~4 times that of the 1s-type states. However, in the above model we show that it is the filtering factor of the detector that dictates how strongly any individual state contributes to the Z-contrast image. It can be seen that the C_{jj} values for the 1s-type states are much larger than all the other states; for a detector with a 26 mrad inner angle the C_{jj} factors are over four times greater and this rises to over two orders of magnitude for a 60 mrad inner angle. These values show that the filtering of the 1s-type states becomes more efficient as the inner angle of the detector is increased. This can also be seen through the reduced background contribution of the other 409-states in the ROF profile (Fig. 3b).

In previous calculations using this approach for GaAs <110>, the 1s state is also the state most excited by a STEM probe positioned over the column. In this calculation we have

Table 1 Calculated values of the excitation and filtering coefficients for <110> InAs with detector inner angles of 26 and 60 mrad and beam energy of 300 keV

State	Excitation	C_{jj}	
		26 mrad	60 mrad
0 (In 1s)	0.193529	0.156097	7.001×10^{-3}
1 (As 1s)	0.244683	0.082966	2.718×10^{-3}
2	0.115214	0.023793	2.710×10^{-5}
3	2.0×10^{-13}	0.022859	3.054×10^{-5}
4 (In 2s)	0.80726	0.022332	5.230×10^{-5}
5	9.2×10^{-13}	3.742×10^{-3}	3.780×10^{-6}
6	0.417664	9.575×10^{-3}	1.180×10^{-5}
7	0.229465	0.013675	2.630×10^{-5}
8	8.2×10^{-13}	8.277×10^{-3}	1.028×10^{-5}
9	0.084823	0.011075	1.752×10^{-5}

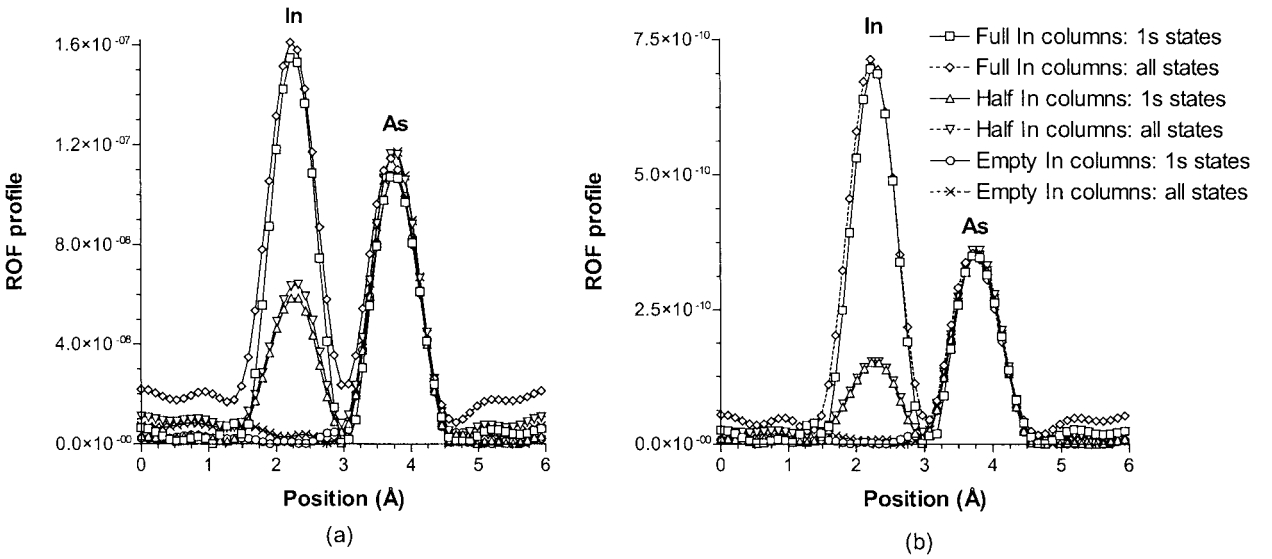

Fig. 4 ROF profiles across the 'dumb-bell' structure with full, half and empty In columns for (a) 26 mrad and (b) 60 mrad inner detector angle.

shown that for a heavier In column, the 2s state will be the most excited and will have a major contribution to the electron density inside the crystal. However, the ADF detector provides a filtering effect represented by the C_{jj} values that means that the 1s states still dominate the ADF image contrast. This filtering effect arises from detecting only the states with a high transverse momentum. This is in contrast to previous calculations [7,8] that calculated integrated intensity over scattering cross sections at the atom sites. For lighter columns, the 1s states will dominate this calculation. For heavier columns, however, the 2s states become bound and highly excited and will not be effectively filtered out. A significant contribution from the 2s states will lead to errors in the thickness dependence of the image intensity because of the difference between the 1s and 2s k_z values. Based on the present results a better simulation would be to calculate the 1s intensity only at the sites, although there is little advantage compared with the present formulation that allows the effects of other states to be included.

Indifference to neighbouring column structure

We have shown that the ROF is dominated by scattering from excited 1s-type Bloch states of the imaged structure, but a single Bloch state is periodic throughout the whole sample. We now need to determine to what extent can we treat the excitation of a 1s Bloch state on a column as being local and independent of neighbouring columns. To do this the Bloch wave calculation of InAs was repeated but this time with both half the number of In atoms in a column and with empty In columns in the structure. Figure 4 shows the ROF profiles across the InAs 'dumb-bell' structure for the three In column structures for detector inner angles of 26 and 60 mrad. The intensity of the As peak in the ROF is invariant under changes to the physical structure of its neighbouring In column. The maximum deviation in the peak intensity of the As column is ~8% and ~1% for the 26 and 60 mrad inner detector angles, respectively, as the In column is completely removed. This shows that we have truly broken the transverse coherence between columns in the formation of a Z-contrast image. Thus, we have a direct structure image of the atomic column positions. We stress that the electron density within the crystal depends on *all* Bloch states, and will, therefore, be strongly affected by the nature of the neighbouring columns. Figure 4 also shows that changing the structure of the In column changes its peak intensity. The variation of the intensity of the In column between full and half In columns varies for the two inner detector angles; the In peak intensity falls by a factor of 0.38 and 0.22 (~¼) for the 26 and 60 mrad inner detector angles, respectively. At high angles the intensity appears to be proportional to the number of atoms squared, as would be expected for coherent scattering. However, experimentally this is not what we would expect since the longitudinal coherence would be broken by phonons.

Cross-talk between columns

When the electron probe is incident on a column of atoms, channelling causes the intensity to be focused tightly on that column but as the thickness increases some intensity can be seen on neighbouring columns as the beam spreads and the wavefunction appears to tunnel between them; this effect is known as 'cross-talk'. However, to understand what types of Bloch states are excited on the neighbouring columns, we need to examine the relationship between the phase ramp, $\mathbf{K}_i.\mathbf{R}_0$, over the incident cone of illumination that controls the probe position and the dispersion surface of the Bloch state eigenvalues, $k_z^{(j)}(\mathbf{K}_i)z$, in eq. (1). This equation shows that if we are to excite the jth Bloch state we have to match the gradients of the linear probe phase ramp and the dispersion surface

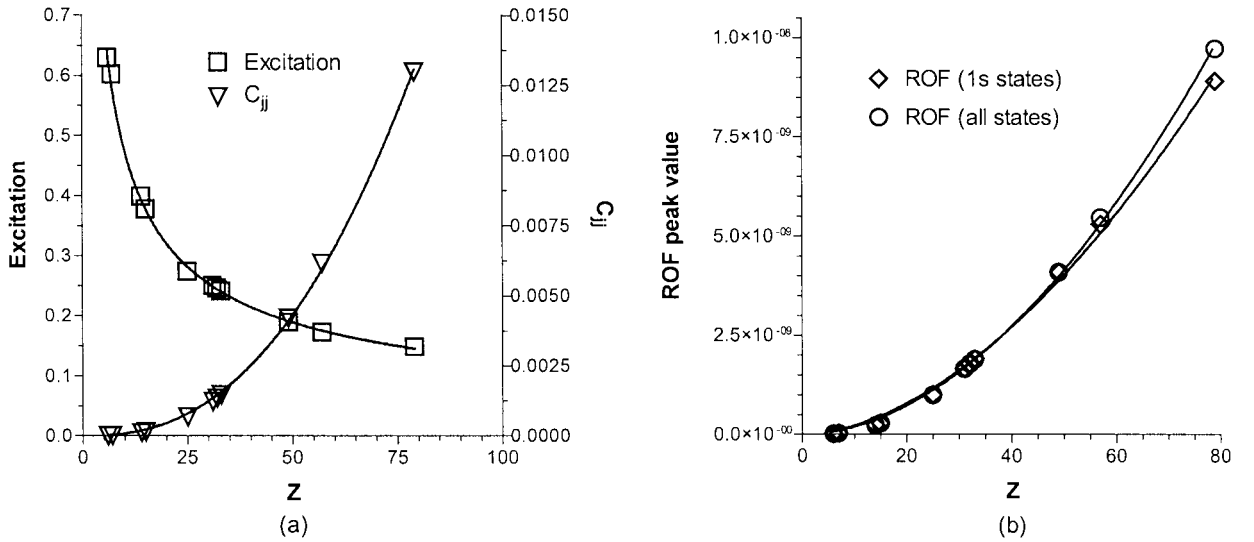

Fig. 5 Plot of (a) the excitation coefficient and C_{jj} parameter for the 1s-type states and (b) the peak intensity of the ROF constructed from the 1s-type states and all states as a function of Z. The curves are the fitted power law dependencies to the data points.

of this Bloch state across the objective aperture, thus,

$$z\frac{\partial k_z^{(j)}}{\partial \mathbf{K}_i} = R_0 \qquad (4)$$

For non-dispersive Bloch states the gradient of the dispersion surface is very close to zero, and eq. (4) is only valid if $R_0 = 0$ for all values of z. Thus, if the probe is not located over the atomic column the 1s Bloch state of this column is not excited, however, other non-1s Bloch states (dispersive states) will be excited. Since we are limited by computing power we have to truncate the number of plane waves used to describe a single Bloch state, thus our 1s-type Bloch states will have a dispersion surface with a non-zero gradient and for some value of z we will satisfy eq. (4) and induce 'cross-talk'. However, using 411-beams there is only a 0.008% change in the value of $k_z^{(1s)}(\mathbf{K}_i)$ moving from the centre of the Brillouin zone to its edge. Therefore, we will only induce 'cross-talk' after the Bloch states have travelled through ~10 μm of crystal. It should also be noted that even with 411-beams the dispersion surface has not completely converged and so this thickness value is a lower limit.

Although the general shapes of the Bloch states can be revealed while using a relatively low number of plane-wave components (~45) [17], this is not nearly enough to obtain full convergence of the Bloch state dispersion surfaces, especially for the non-dispersive states, and this has significant consequences to the 'cross-talk' between neighbouring columns. The calculations carried out in this paper typically used between 400 and 800 plane-wave components* with an error of ~ 5% and ~1%, respectively.

Dependence of the image contrast on column composition

To investigate the Z-dependence of the ROF, calculations were performed for eleven different elements with a range of Z values (Z = 6 (carbon) to Z = 79 (gold)). The unit cell of InAs was used with the atoms placed on the In sites only (the As sites being left empty). The calculations were also expanded to include 781 Bloch states, each with 781 plane-wave components, to ensure convergence and adequate sampling of reciprocal space at high angles. Figure 5a shows a plot of the on-axis excitation and filtering factor for a 60 mrad inner detector angle as a function of Z. Figure 5b shows the column peak intensity values of the corresponding ROFs constructed with just the 1s-type Bloch states and all 781 Bloch states. It is assumed that these parameters have a power law dependence ($A \times Z^n$), which has been fitted to the data points (see curves in Fig. 5 and Table 2). It is clear that the high-angle limit of the ROF intensity approaches the Z-dependence expected for screened Rutherford scattering, with a value of $n = 1.77 \pm 0.05$ and $n = 1.88 \pm 0.03$ for the 1s-type states and all states, respectively.

Table 2 A summary of the results of the power law fitting to the data points in Fig. 5

	Excitation	C_{jj}	ROF peak intensity	
			1s states	all states
n	–0.5762	2.419	1.770	1.880
σ	0.008406	0.03694	0.04579	0.03147

*Since the filtering factor C_{jj} is very sensitive to high angle contributions from Bloch states, this was used to test for convergence in the Bloch wave calculations.

Concluding remarks

We have shown that even in the presence of dynamical scattering the geometry of the detector is responsible for the filtering of the highly localized 1s-type Bloch states and is the source of the transverse incoherence of a Z-contrast image. This has been further demonstrated by the indifference of column peak intensities to the structure and composition of its neighbouring columns. This result is not dependent on the presence of phonon scattering to break transverse coherence, although this is important in breaking longitudinal coherence, which we shall explore further in a future paper. We have also shown that in the limit of a large inner detector angle the dynamical image contrast approaches the classical screened Rutherford Z^2 dependence, which would be anticipated for single atom scattering. It is an interesting result that using a high-angle detector selects electrons in the high transverse momentum dynamical 1s state, which gives the same Z-dependence as scattering from a single atom albeit with a much increased intensity.

The important conclusion from this work is that simply computing the electron intensity within the crystal can be misleading with regard to how the ADF image contrast is actually formed. For heavier columns illuminated by a STEM probe the 2s state will be the most excited, resulting in a major contribution to the electron intensity, but we have shown that the contribution of the 2s state to the ADF image contrast is negligible compared to the 1s states. This is clearly an important conclusion since many previous approaches to ADF image simulation have used integrations of the electron intensity over scattering cross-sections at the atom sites.

It is also well known that the elastic scattering and propagation within the crystal leads to broadening of the probe as it propagates through the crystal. However, this Bloch wave analysis demonstrates that the broadening occurs through *non*-1s states since the 1s states are non-dispersive. Because the 1s states dominate the ADF contrast, this dechannelling of the probe into neighbouring columns does not destroy the transverse incoherence of the imaging process. The atomic columns remain as independent incoherent scattering centres with no cross-talk.

Acknowledgements

This research was supported by Oak Ridge National Laboratory, managed by UT-Battelle, LLC, for the U.S. Department of Energy under contract DE-AC05-96OR22725, and by appointments to the ORNL Postdoctoral Research Associates Program, administered jointly by ORNL and ORISE. P. D. Nellist is grateful to The Royal Society (London) for financial support. We are also grateful to the University of Bristol (UK) Microstructures Group for supplying the code for performing the Bloch wave simulations.

References

1 Chisholm M F, Maiti A, Pennycook S J, and Panfelides S T (1998) Atomic configurations and energetics of arsenic impurities in a silicon grain boundary. *Phys. Rev. Lett.* **81**: 132–135.

2 McGibbon M M, Browning N D, Chisholm M F, McGibbon A J, Pennycook S J, Ravikumar V, and Dravid V P (1994) Direct determination of grain-boundary atomic-structure in $SrTiO_3$. *Science* **266**: 102–104.

3 McGibbon A J, Pennycook S J, and Angelo J E (1995) Direct observation of dislocation core structures in CdTe/GaAs(001). *Science* **269**: 519–521.

4 Dickey E C, Dravid V P, Nellist P D, Wallis D J, and Pennycook S J (1998) Three-dimensional atomic structure of NiO-ZrO_2(cubic) interfaces. *Acta Mat.* **46**: 1801–1816.

5 Nellist P D and Pennycook S J (1998) Accurate structure determination from image reconstruction in ADF STEM. *J. Microsc.* **190**: 159–170.

6 Treacy M M J, Howie A, and Wilson C J (1978) Z contrast imaging of platinum and palladium catalysts. *Phil. Mag. A* **38**: 569–585.

7 Pennycook S J and Jesson D E (1990) High-resolution incoherent imaging of crystals. *Phys. Rev. Lett.* **64**: 938–941.

8 Pennycook S J and Jesson D E (1991) High-resolution Z-contrast imaging of crystals. *Ultramicroscopy* **37**: 14–38.

9 Jesson D E and Pennycook S J (1995) Incoherent imaging of crystals using thermally scattered electrons. *Proc. Roy. Soc. (London) A* **449**: 273–293.

10 Jesson D E and Pennycook S J (1993) Incoherent imaging of thin specimens using coherently scattered electrons. *Proc. Roy. Soc. (London) A* **441**: 261–281.

11 Loane R F, Xu P, and Silcox J (1992) Incoherent imaging of zone-axis crystals with ADF STEM. *Ultramicroscopy* **40**: 121–138.

12 Nellist P D and Pennycook S J (1999) Incoherent imaging using dynamically scattered coherent electrons. *Ultramicroscopy* **78**: 111–124.

13 Humphreys C J and Bithell E G (1992) Electron diffraction theory. In: *Electron Diffraction Techniques*, Vol. 1, ed. Cowley J M, pp. 75–151 (Oxford University Press, Oxford).

14 Amali A and Rez P (1997) Theory of lattice resolution in high-angle annular dark-field images. *Microsc. Microanal.* **3**: 28–46.

15 Spence J C H, Zuo J M, and Lynch J (1989) On the HOLZ contribution to STEM lattice images formed using high-angle dark-field detectors. *Ultramicroscopy* **31**: 233–240.

16 Nellist P D and Pennycook S J (2000) The principles and interpretation of annular dark-field Z-contrast imaging. *Adv. Imag. Electron Phys.* **113**: 147–207.

17 Fertig J and Rose H (1981) Resolution and contrast of crystalline objects in high-resolution scanning transmission electron microscopy. *Optik* **59**: 407–429.